Inverted Stripline Antennas Integrated with Passive and Active Solid-State Devices

Julio A. Navarro, *Member, IEEE*, and Kai Chang, *Fellow, IEEE*

Abstract—**Integrated antennas can reduce the size, weight, and cost of many microwave systems by incorporating component functions directly at the antenna terminals. Their use in many commercial system applications can produce compact, low-cost products. Currently, active integrated antennas are used for distributed oscillators in spatial and quasi-optical power combining. The inverted stripline antenna configuration was developed to easily integrate with solid-state diodes or transistor devices for switching, tuning, modulation, amplification, and oscillating functions. This antenna configuration offers good performance, beam sharpening flexibility, and nondestructive optimization. Good switching, tuning, and oscillating performances have been demonstrated.**

I. Introduction

OVER THE last few years, integrated antennas have received a great deal of attention because they can reduce the size, weight and cost of many transmit and receive systems [1]. Passive and active solid-state devices can be used to combine several component functions at the terminals of the antenna. For example, active devices can be used to design active integrated antenna oscillators, amplifiers and multipliers. These active integrated antennas are ideal for current investigations in spatial and quasi-optical power combining. Integrated antennas pose an interesting problem involving several different areas of microwave engineering such as solid-state devices, circuits, components and antennas. Knowledge of solid-state device characteristics and circuit integration are critical as well as component specifications and antenna performance.

Combining guided-wave circuits with radiating structures often leads to several trade-offs in performance. Material properties which enhance circuit performance often degrade antenna radiation. DC biasing circuits and device packages also disturb antenna characteristics. Similarly, an antenna's radiation may degrade a component's performance. These difficulties need to be overcome so that integrated antennas are able to meet system requirements in military and commercial applications.

Solid-state devices such as two-terminal diodes and three-terminal transistors are small, light-weight and easy to reproduce. These devices are used to develop switching [2], tuning [3]–[5], detecting [6], mixing [7], amplifying [8] and oscillating components. The choice of device depends on the type of microwave component, operating frequency, power output and other considerations. Although transistors offer higher dc-to-RF conversion efficiencies, diodes reach higher operating frequencies and power levels. Diodes normally need higher dc input levels but transistors require more complicated biasing schemes. The choice of solid-state device for an integrated antenna also involves its effect on the radiation characteristics. Although integrated antennas can reduce the size, weight and cost of many microwave systems, active integrated antennas have shown a deterioration of both the antenna and component performance. If an integrated antenna can maintain component specifications with little degradation in the radiation characteristics, the approach would be very attractive for many commercial and military systems.

For the past decade, integrated antennas have mainly focused on active microstrip patches [9]–[16] for radiators in power combining applications. The patch serves as the resonator which compensates for the active device's reactance at the oscillation frequency. The diode position along the antenna determines operating frequency, output power and radiation performance. Analytical models and commercial software packages can calculate resonant frequencies and input impedance along the length of the patch which can be used to find an optimum position for a solid-state device. These models, however, seldom account for device packages, biasing lines and integration discontinuities which disrupt the fields and currents of the antenna. These disturbances often cause changes in operating frequencies, lower conversion efficiencies and higher cross-polarization levels (CPL). Variations in circuit dimensions, dielectric characteristics and diode parameters also introduce errors in the final design. These errors are typically tuned out after assembly in order to consistently meet frequency and power specifications.

The ability to integrate shunt devices easily is of particular importance for active applications. Shunt connections in microstrip requires drilling in MIC's and via hole processing in monolithic MIC's. Some alternative uniplanar geometries have been demonstrated for active and integrated antennas [17]–[22]. Uniplanar transmission lines such as coplanar waveguide, slotline and coplanar strips do not require drilling for shunt connections alleviating the hybrid integration discontinuities encountered in microstrip.

Although not a true uniplanar line, inverted microstrip does not require drilling for shunt connections. This allows nondestructive experimental testing as well as position optimization of diodes and coaxial probe inputs. This trait makes inverted microstrip attractive for hybrid applications. When used for integrated antennas, inverted microstrip provides a

Manuscript received September 12, 1994; revised May 25, 1995. This work was supported in part by NASA-Lewis Research Center in Cleveland, OH, the U. S. Army Research Office, and the Texas Higher Education Coordinating Board's Advanced Technology Program.

The authors are with the Department of Electrical Engineering, Texas A&M University, College Station, TX 77843-3128 USA.

IEEE Log Number 9413420.

built-in radome for protection. By carefully matching the thermal expansion and conductivity coefficients of substrate materials and housing alloys, the integrated antenna can also be hermetically sealed for improved system durability and reliability [23], [24]. DC biasing of devices can be achieved on the substrate or through the ground plane underneath. For increased metal volume and isolation, the antenna is enclosed by a metallic enclosure which can then be classified as trapped inverted microstrip. However, this is a special case of general stripline-type configurations [25].

Gunn-integrated active inverted stripline antennas have been demonstrated in [26], [27] for beam steering and spatial power combiners. These active antennas exhibit good radiation patterns, low cross-polarization levels, easy device integration and good heat sinking capacity. Furthermore, this configuration is useful in passive probe-fed applications as well as integration with FET's and other devices.

In this paper, a cavity model is used to calculate the resonant frequencies of the inverted configuration and compared to measured results. A novel test fixture was devised to nondestructively determine input impedance as a function of probe position. The fixture also allows testing of different antenna dimensions, cavity diameters and substrate dielectric constants and thicknesses. Switchable and tunable probe-fed antennas were demonstrated using PIN's and varactor diodes, respectively. An FET integrated inverted stripline antenna was also developed with excellent oscillation and radiation performance.

II. Design and Test of Passive Antennas

The inverted microstrip configuration removes the ground plane from the substrate backside and inverts the conductor over a ground plane support. The electromagnetic fields are primarily concentrated in the air between the patch and the ground plane providing a lower effective dielectric constant (ε_{eff}), a longer guided wavelength and higher characteristic impedance over a comparable line width in microstrip. Although series or shunt devices are easy to integrate, the inverted configuration is prone to exciting surface wave modes. Surface waves cause considerable cross-talk in densely packed circuits, reduce radiation efficiency and distort antenna patterns. Shorting pins or metallic walls to either side of the conductor can eliminate these unwanted modes. The patch antenna in this configuration can be etched with an arbitrary shape while a circular enclosure is more easily manufactured. In this investigation, circular patch antennas were used to maintain circular symmetry. This structure can be classified as a trapped inverted microstrip which is a subset of the more general stripline-type transmission lines.

Fig. 1 shows the top and side view of the inverted stripline antenna (ISA) configuration. The important dimensions are shown as well as the novel test fixture. These dimensions are used to determine an effective diameter for the patch antenna

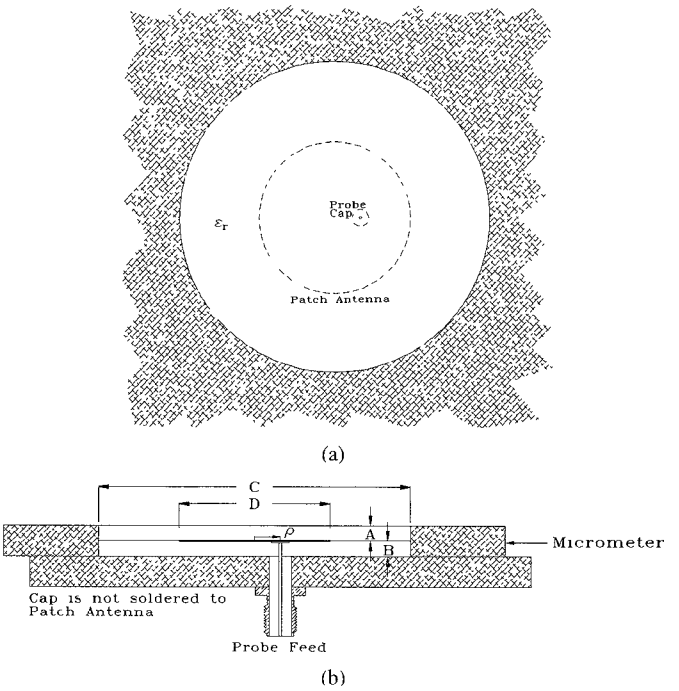

Fig. 1. Configuration of the inverted stripline antenna (ISA) and test fixture (a) top view, (b) side view.

and the corresponding resonant frequency (F_o). Using a conventional cavity model the resonant frequency is calculated using [28]

$$F_o = \frac{\alpha_{mn} c}{\pi D_{\text{eff}} \sqrt{\varepsilon_{\text{eff}}}} \tag{1}$$

where c is the speed of light, α_{mn} is 1.84118 for the dominant mode and D_{eff} is the effective patch diameter due to fringing fields over the radiating edges given by [29] as shown in (2) at the bottom of the page, where D is the physical patch diameter and the height (B) is the patch-to-ground separation. The substrate used is RT-Duroid 5870 with an $\varepsilon_r \approx 2.3$. In this configuration, the majority of the fields are concentrated within the region defined by the patch and the ground plane. Since air fills the region below the patch, the effective dielectric constant (ε_{eff}) is very nearly one. An empirically determined value of 1.1 gives resonant frequency values within 3% of the measured results which range from 3–12 GHz.

As shown in Fig. 1, the dielectric substrates are cut in 62 mm circular inserts. The inserts are press-fitted on a 3 mm deep, ~62 mm cavity enclosure. The inserts are suspended approximately 1.5 mm above the ground plane housing. The ground plane housing has a coaxial probe-feed topped by a 3.5 mm diameter cap which ensures good contact with the antenna and avoids soldering. The probe input was connected to an HP-8510B Network Analyzer and calibrated up to the antenna ground plane. The analyzer tests input impedance match, operating frequency and impedance bandwidth.

This configuration and test fixture allows the enclosure and substrate insert to slide over the probe feed for position

$$D_{\text{eff}} = \frac{D}{2}\sqrt{1 + \left(\frac{4B}{\pi \cdot D \cdot \varepsilon_{\text{eff}}}\right)\left(\ln\left(\frac{D}{4B}\right) + 1.77 + 1.41\varepsilon_{\text{eff}} + \frac{2B}{D}(0.268\varepsilon_{\text{eff}} + 1.65)\right)} \tag{2}$$

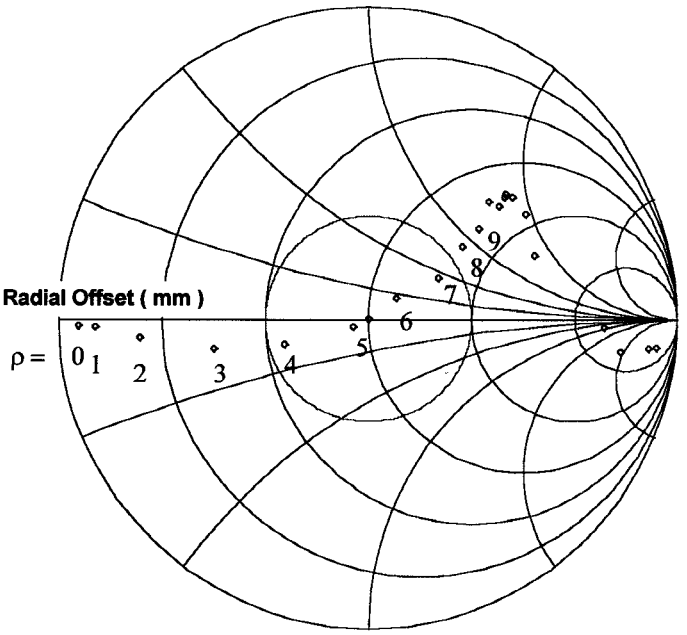

Fig. 2. Input impedance versus radial offset ρ for patch diameters $D = 30$ mm; other parameters are $C = 62$ mm, $A = 1.5$ mm, and $B = 1.5$ mm. The dotted line denotes the 2:1 VSWR circle.

optimization. Accurate probe position is measured with a micrometer. Fig. 2 shows the ISA input impedance of the fundamental mode versus probe position from the center for a 30 mm diameter patch. The best 50 Ω input match for this antenna occurs at 5.21 mm where the VSWR is 1.0003 and the 2:1 bandwidth is 3.77%. As shown, the probe can be positioned over a fairly wide range and it still maintains a 2:1 VSWR. The dominant mode appears as a short circuit at the center of the patch and increases in impedance at the edge of the antenna. Similar results were obtained for other patch diameters.

Different substrate inserts with patch antenna diameters which varied from 10–60 mm were optimized for best 50 Ω match at the operating frequency. Fig. 3 shows measured versus calculated operating frequencies of the ISA structure as a function of patch diameter. The calculations are accurate to within a few percent of the measured results. For the structure dimensions of this investigation, the operating frequencies are primarily determined by the patch size and patch-to-ground separation. These operating frequencies are typically some distance away from the nearest cavity mode which should not pose any problems. Similar results have been reported in [30]. Errors may be due to variations in patch-to-ground separation, probe discontinuities and metallic wall effects on the antenna radiating edges. Also shown in Fig. 3 is the VSWR for each antenna diameter. As the probe moves along the patch, the reflection coefficient (S_{11}) can be optimized for best 50 Ω match. S_{11} levels less than −25 dB were obtained for each antenna. Fig. 4 shows 2:1 impedance bandwidths versus patch diameters. As shown, the 2:1 impedance bandwidth is dependent on the patch to cavity diameter ratio. Large bandwidths are possible using a simple probe-feed without complex matching circuits. The bandwidth increase for smaller patch dimensions is expected since the separation (B) is larger with respect to the wavelength of operation.

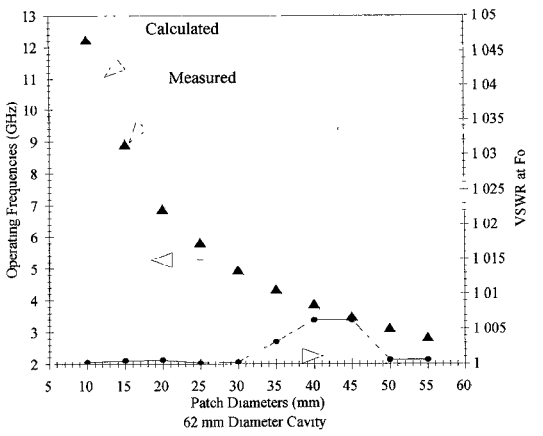

Fig. 3. Operating frequency versus patch diameters.

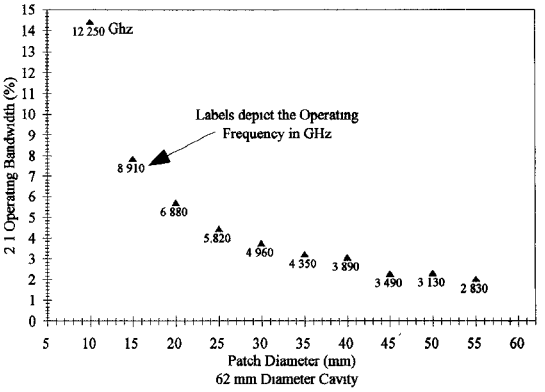

Fig. 4. 2:1 input impedance bandwidth versus patch diameters.

The radiation patterns were tested using an HP automated antenna test system. The radiation patterns for the 30 mm diameter antenna are shown in Fig. 5. The E- and H-plane half-power beamwidths (HPBWs) are 57.5 and 61.5°, respectively. The cross-polarization level is 19.3 dB below the measured gain of 10.5 dBi. Radiation patterns for other patch diameters show that the HPBW varies with the patch-to-cavity diameter ratio. Fig. 6 shows the HPBWs of the E- and H-plane patterns of several antennas tested in the 62 mm diameter cavity. The inverted substrate and enclosure combination increase the antenna directivity. Noticeable beam sharpening occurs near patch-to-cavity diameter ratios of ≈ 0.5.

As shown in this section, the inverted configuration offers good circuit and antenna performance and it has flexibility in operating bandwidth and radiating beamwidth. Just as the coaxial probe was moved under the antenna, solid-state device positions can also be optimized for best impedance match. The following sections describe integrations with PIN, varactor, Gunn diodes and FET's for hybrid MIC applications.

III. Integrated Antennas with PIN's and Varactors

Two-terminal device integration for this structure is straightforward. Diodes can be connected across the patch to ground. Fig. 7(a) shows integration with two PIN or varactor diodes. From Fig. 7(a), varying the diode position under the patch changes the impedance seen by the diode. Alternatively, the diode position determines the diode's effect on the antenna. Since the electric field is a maximum at the radiating edges

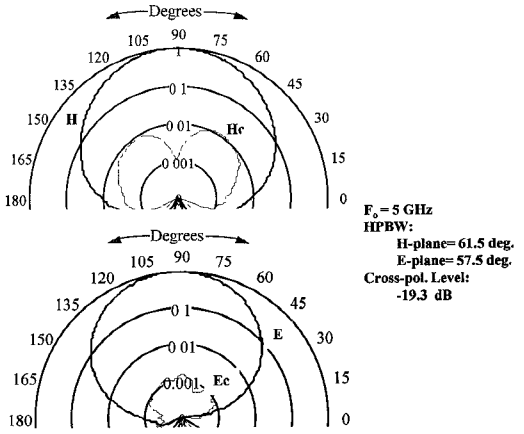

Fig. 5. E- and H-plane radiation patterns for $D = 30$ mm.

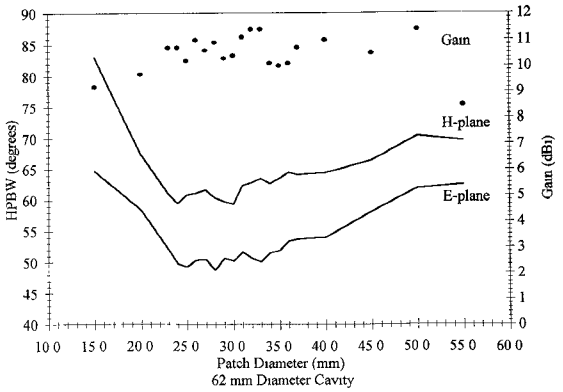

Fig. 6. Measured gain and E- and H-plane HPBW's versus patch diameters.

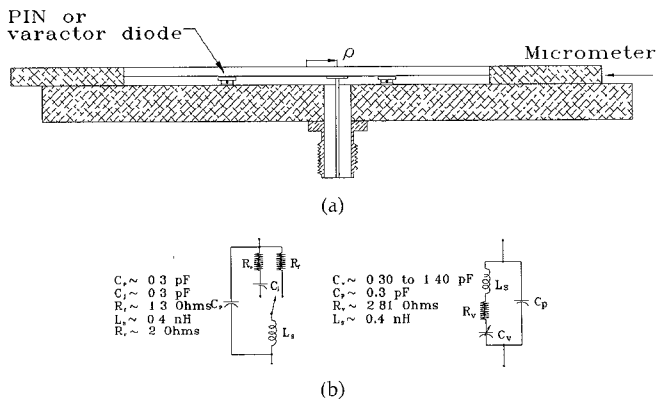

Fig. 7. (a) ISA integrated with PIN or varactor diodes. (b) Equivalent circuit of PIN and varactor diodes.

of the antenna, PIN and varactor diodes will have the most effect at these positions. Equivalent circuits for PIN and varactor diodes are shown in Fig. 7(b). The packaged diodes are soldered to the patch at the radiating edges and the antenna detuning is compensated by slightly adjusting the probe position.

PIN diodes switch electronically between two states which can be used to turn the antenna fundamental mode on and off. At zero bias, the PIN behaves as a load which lowers the antenna operating frequency from 4.96–4.12. Smaller diode packages and positions away from the radiating edges reduce this effect. As the bias is increased from 0–1 Volt, the PIN diodes short circuit the radiating edges of the patch effectively

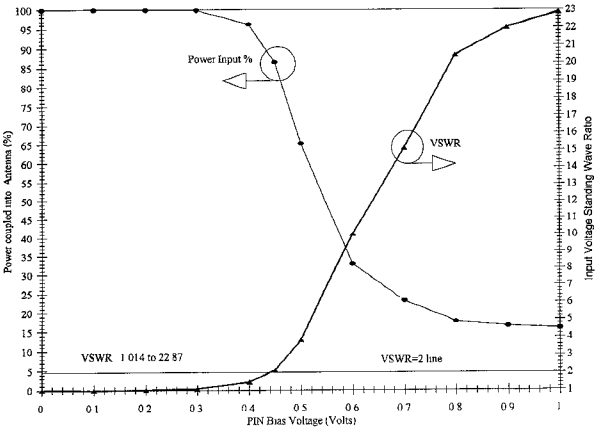

Fig. 8. PIN switching on ISA input VSWR versus bias for $D = 30$ mm.

switching the antenna off. By varying the bias voltage, the antenna reflection coefficient at the operating frequency varies from a VSWR of 1.014–22.87 as shown in Fig. 8. When the diodes are not biased, the VSWR is 1.014. At 1 V (100 mA), the VSWR is 22.87. This effect can be used for switching and amplitude modulation. The power coupling into the antenna is also shown in Fig. 8. The diodes used in this investigation are M/ACOM's general purpose PIN diodes housed in case style #32. The performance would be improved with better diode characteristics and smaller case styles.

If varactors are used instead of PIN diodes, the operating frequency is shifted or tuned with respect to the varactor bias voltage. The M/ACOM varactors used are abrupt junction diodes also housed in case style #32. The varactor capacitance varies as a function of bias voltage (V) according to

$$C(V) = \frac{C(0)}{\left(1 + \frac{V}{V_{bi}}\right)^{\gamma}} \tag{3}$$

where $C(0)$ is the capacitance at 0 Volts, V_{bi} is the built-in potential (GaAs = 1.3 V) and γ is 0.5 for abrupt junctions.

Varactor diodes will have maximum effect on the antenna if they are placed at electric field maxima. At the radiating edges, the varactors couple very strongly with the radiating electric field loading the antenna and lowering the operating frequency. When biased, the varactors can quickly tune over a range of frequencies. Varactor integrated antennas have exhibited a 2:1 VSWR tuning range of over 31% centered at 3.4 GHz. As shown in Fig. 9, at 30 V the operating frequency is at 3.88 GHz with a VSWR of 1.0105. At 0 V the operating frequency is at 2.84 GHz with a VSWR of 1.0053. Fig. 10 shows the ISA 2:1 impedance bandwidth and VSWR versus operating frequency. As shown, the VSWR remains below 1.02 while the impedance bandwidth varies from 1.8–2.5%. This integrated antenna can be used to rapidly scan over its tuning bandwidth for wideband receiver or transmitter applications. The small instantaneous bandwidth (~2%) reduces noise figure in a wideband antenna receiver system.

As in all integrated antennas, there is a degradation in radiation performance due to antenna modifications and device perturbation of the antenna fields. For example, the cross-polarization for the varactor integrated patch is −10 dB compared to −19 dB for the nonintegrated patch. Smaller

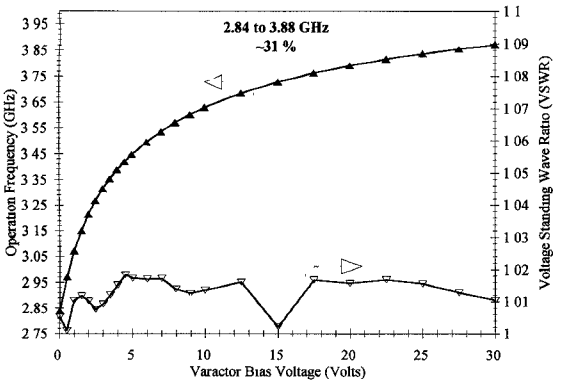

Fig. 9. Varactor tuning on ISA operating frequency versus bias for D = 30 mm.

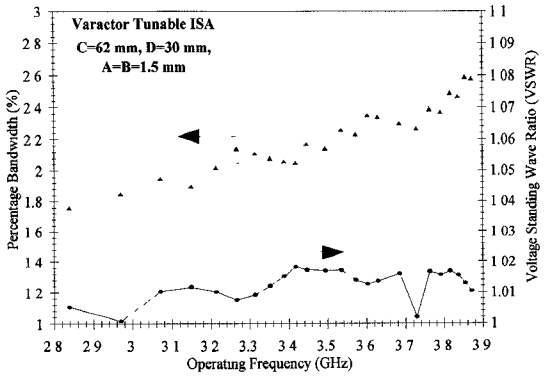

Fig. 10. Varactor tuning on ISA impedance bandwidth and VSWR versus operating frequency.

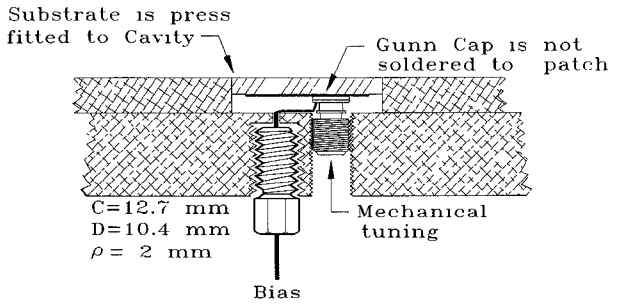

Fig. 11. Gunn integrated ISA in adjustable test fixture.

devices, improved biasing schemes and optimized diode positions will reduce the effect on the radiation pattern.

IV. Active Antennas Using Gunn Devices

Unlike PIN- and varactor-integrated antennas, Gunn integrated antennas generate RF power output. The antenna serves as the resonator as well as the radiator for the oscillator. Oscillations occur at the frequency where the diode and the antenna reactances cancel out. Oscillation startup occurs if the placement of the diode is such that the magnitude of the diode negative resistance is greater than the circuit resistance presented to its terminals. Fig. 11 shows the Gunn integrated ISA in the adjustable test fixture. The package connection to the heat sink and the added metal volume of the metallic walls provide efficient heat sinking for the active device.

M/ACOM 49106-111 diodes were integrated with antennas ranging from 8–11 mm in diameter. The smaller antenna

TABLE I
Gunn Integrated ISA Operating Frequencies, Power Versus Diameter

Patch Diameter (mm)	Measured Fo (GHz)	Oscillator Power* (mW)
8	9.997	63.99
9	9.637	56.76
10	9.438	57.04
10.4	9.240	63.98
11	8.908	66.98

* Calculated using a passive antenna gain of 6.65 dBi. Cavity diameter is 12.7 mm.

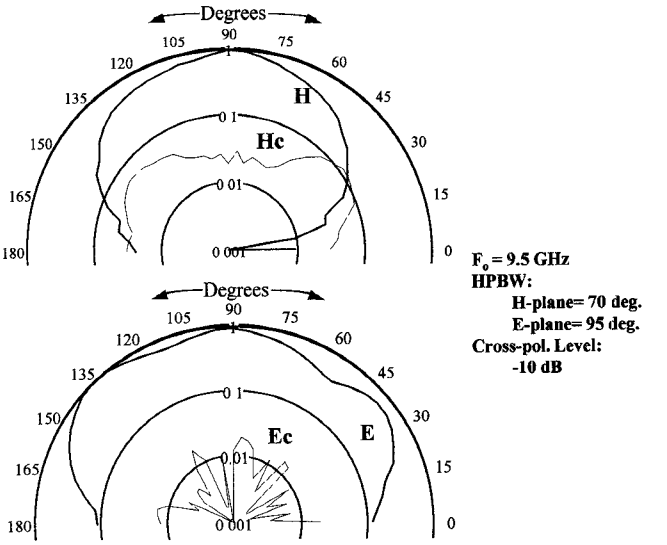

Fig. 12. Gunn integrated ISA radiation patterns.

diameters are used for X-band operation. Since active antennas are mainly intended for use in spatial and quasi-optical power combining, packing density is important. To increase packing density, the metallic walls of the enclosure are very near the edges of the antenna. The diode package as shown in Fig. 11 presents a significant perturbation on the X-band antenna volume which adversely affect the radiation characteristics and disturb the oscillating frequency. The Gunn oscillator frequency and de-embedded power outputs are listed in Table I. The power output is calculated using the Friis transmission equation [12].

Radiation patterns for the Gunn integrated ISA are shown in Fig. 12 [27]. The cross polarization level is at least −10 dB for a Gunn diode 2 mm off-center. The HPBWs are 100 degrees in the E-plane and 70 degrees in the H-plane. A similar antenna using a probe feed exhibited HPBWs of 105 and 80 degrees in the E- and H-plane, respectively with a cross-polarization level of −16 dB. The differences in radiating performance are attributed to the active antennas' diode package and bias lines. Improved performance can be achieved by reducing the size of the device packages. The HPBW's of the X-band ISA's and those of Section II differ because of device and probe perturbation effects and differences in cavity depth and ground plane size with respect to wavelength.

V. Active Antennas with FET's

The use of the FET transistor improves conversion efficiency and noise characteristics while it reduces thermal requirements. However, the antenna must be modified to acco-

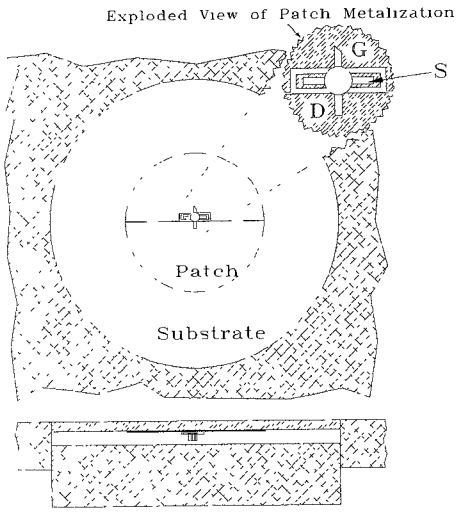

Fig. 13. FET integrated ISA configuration.

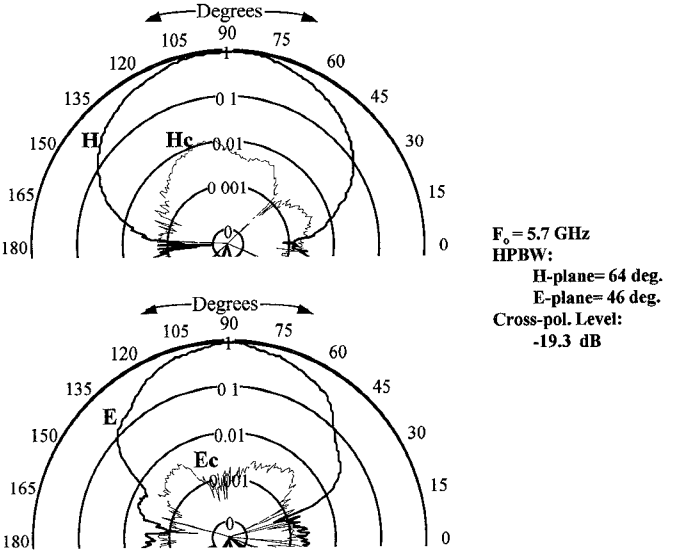

Fig. 14. FET integrated ISA antenna radiation patterns.

modate the FET as shown in Fig. 13. FET integration requires three dc blocks for the drain, gate and source terminals. DC biasing can be achieved from behind the ground plane or etched to the nonradiating edges of the antenna. A chip resistor connected across the source to gate simplifies biasing to the device. The operating frequency is determined by the loads at each transistor port. The transistor can be induced to oscillate at lower frequencies to reduce effects from the device package and bias lines. Lower frequencies of operation can be accomplished with larger patch diameters.

A 30 mm patch was modified to insert the FET (NEC model 76184A). At the center of the patch, 0.4 mm gaps isolate the source from the gate and drain terminals. A 0.1 mm gap is etched from the center to the nonradiating edges of the patch to provide dc isolation between the gate and drain terminals. The FET drain lead is soldered at the center of the patch and the gate lead is approximately 2 mm off-center. Three dc lines bias the source, gate and drain of the transistor. Alternatively, the source bias line can be replaced by a resistor. The frequency of oscillation depends on the impedance loads at the FET ports. The loads are a function of the position along the inverted patch antenna. Heat generated is dissipated by the patch. The lack of a low-impedance path from the device to the metal heat sink may cause thermal problems in higher power devices. This could be alleviated with a shorting pin at the center of the patch to provide a low impedance path to the housing.

Since the antenna was modified and the device terminal are soldered, it is not possible to experimentally optimize the FET position. However, a ground plane sliding short is used to change the antenna cavity depth and alter the oscillation frequency. The cavity depth is used to improve spectral and radiation characteristics of this active antenna.

The FET provides 57 mW at 5.69 GHz when biased at 3.8 V and 26 mA. The 3 dB bias tuning range is approximately 1% for a 1 V change in v_{ds}. The sliding ground plane allows a mechanical tuning range of nearly 6%. At a cavity depth of 4.15 mm, the measured oscillation frequency remains stable at 5.695±0.002 GHz over the antenna test sweep. The HPBW in the E- and H-plane patterns are 46 and 64°, respectively. The cross-polarization level is −19.3 dB below the maximum. Fig. 14 shows principal plane and cross-polarization patterns of the active antenna. The smooth radiation patterns and low cross-polarization level compares favorably with previously reported active antennas [9]–[13], [15]. Probe-fed passive antennas with cavity depths of 3 mm exhibited HPBWs of 51 and 61° in the E- and H-plane patterns, respectively. The cross-polarization level of the passive antenna is also −19.3 dB with a gain of 10.2 dBi. Biasing modifications and cavity depth differences in the active antenna may account for the changes. The effective isotropic radiated power of the active antenna is 594 mW. Approximating the active antenna gain with the passive antenna gain of 10.2 dB results in an oscillator power of 57 mW and a dc-to-RF conversion efficiency of 57%.

VI. Conclusion

A useful passive inverted stripline antenna configuration has been demonstrated. Integration has been demonstrated with PIN and varactor diodes with some degradation of the antenna performance. The integration creates switchable and tunable radiating MIC components. Gunn diodes have also been integrated for active antenna radiators with good output power and a clean spectrum. An FET has shown very good oscillator characteristics as well as exceptional radiation performance. It operates at low voltage and current levels with high conversion efficiency. These active antennas can be used for doppler sensing [31], disposable decoys, wireless communications, phased-arrays [26], [32] and power combining applications. Overall, these integrated and active integrated antennas perform well as compared to current state-of-the-art passive radiators. Further improvement can move these components closer to commercial applications. Combinations of several devices will allow the ability to integrate various component functions.

Acknowledgment

The authors would like to thank the Rogers Corporation for the substrate material which they provided, as well as L. Fan and J. McSpadden for their technical support.

REFERENCES

[1] D. B. Rutledge, D. P. Neikirk, and D. P. Kasilingam, "Integrated circuit antennas," in *Infrared and Millimeter-Waves,* K. J. Button, ed., chap. 1, vol. 10. New York: Academic, 1983, p. 25.

[2] R. B. Waterhouse and N. V. Shuley, "Dual frequency microstrip rectangular patches," *Electron. Lett.,* vol. 28, no. 7, pp. 606–607, Mar. 26, 1992.

[3] P. Bhartia and I. J. Bahl, "Frequency agile microstrip antennas," *Microwave J.,* vol. 25, pp. 67–70, Oct. 1982.

[4] P. M. Haskins, P. S. Hall, and J. S. Dahele, "Active patch antenna element with diode tuning," *Electron. Lett.,* vol. 27, no. 20, pp. 1846–1847, Sept. 26, 1991.

[5] M. P. Purchine, J. T. Aberle, and C. R. Birtcher, "Tunable L-band circular microstrip patch antenna," *Microwave J.,* pp. 80–88, Oct. 1993.

[6] S. S. Gearhart, C. C. Ling, and G. M. Rebeiz, "Integrated millimeter-wave corner-cube antennas," *IEEE Trans. Antennas Propagat.,* vol. AP-39, no. 7, pp. 1000–1006, July 1991.

[7] C. M. Jackson, "Patch antenna quasi-optical mixers," *Microwave Opt. Technol. Lett.,* vol. 1, no. 1, pp. 1–4, Mar. 1988.

[8] B. Robert, T. Razban, and A. Papiernik, "Compact amplifier integration in square patch antenna," *Electron. Lett.,* vol. 28, no. 14, pp. 1808–1810, Sept. 10, 1992.

[9] H. J. Thomas, D. L. Fudge, and G. Morris, "Gunn source integrated with a microstrip patch," *Microwaves and RF,* pp. 87–89, Feb. 1985.

[10] T. O. Perkins, "Active microstrip circular patch antenna," *Microwave J.,* pp. 109–117, Mar. 1987.

[11] K. Chang, K. A. Hummer, and G. Gopalakrishnan, "Active radiating element using FET source integrated with microstrip patch antenna," *Electron. Lett.,* vol. 24, no. 21, pp. 1347–1348, Oct. 13, 1988.

[12] K. Chang, K. A. Hummer, and J. Klein, "Experiments on injection locking of active antenna elements for active phased arrays and spatial power combiners," *IEEE Trans. Microwave Theory Tech.,* vol. 37, no. 7, pp. 1078–1084, July 1989.

[13] J. Birkeland and T. Itoh, "FET-based planar circuits for quasi-optical sources and transceivers," *IEEE Trans. Microwave Theory Tech.,* vol. 37, no. 9, pp. 1452–1459, Sept. 1989.

[14] K. D. Stephan and S. Young, "Mode stability of radiation-coupled interinjection-locked oscillators for integrated phased arrays," *IEEE Trans. Microwave Theory Tech.,* vol. 36, no. 5, pp. 921–924, May 1988.

[15] R. A. York and R. C. Compton, "Quasi-optical power combining using mutual synchronized oscillator arrays," *IEEE Trans. Microwave Theory Tech.,* vol. 39, no. 6, pp. 1000–1009, June 1991.

[16] X. D. Wu, K. Leverich, and K. Chang, "Novel FET active patch antenna," *Electron. Lett.,* vol. 28, no. 14, pp. 1853–1854, Sept. 24, 1992.

[17] U. Guttich, "Planar integrated 20 GHz receiver in slotline and coplanar waveguide technique," *Microwave Opt. Technol. Lett.,* vol. 2, no. 11, pp. 404–406, Nov. 1989.

[18] Z. B. Popovic, R. M. Weikle II, M. Kim, K. A. Potter, and D. B Rutledge, "Bar-grid oscillators," *IEEE Trans. Microwave Theory Tech.,* vol. 38, no. 3, pp. 225–230, Mar. 1990.

[19] J. A. Navarro, Y. Shu, and K. Chang, "Broadband electronically tunable planar active radiating elements and spatial power combiners using notch antennas," *IEEE Trans. Microwave Theory Tech.,* vol. 40, no. 2, pp. 323–328, Feb. 1992.

[20] W. K. Leverich, X. D. Wu, and K. Chang, "New FET active notch antenna," *Electron. Lett.,* vol. 28, no. 24, pp. 2239–2240, Nov. 19, 1992.

[21] X. D. Wu and K. Chang, "Compact wideband integrated active slot antenna amplifier," *Electron. Lett.,* vol. 29, no. 5, pp. 496–497, Mar. 4, 1993.

[22] H. P. Moyer and R. A. York, "Active cavity-backed slot antenna using MESFET's," *IEEE Microwave and Guided Wave Lett,* vol. 3, no. 4, pp. 95–97, Apr. 1993.

[23] S. Sanzgiri and J. Tolleson, "Ka band sub-array technology demonstration program," *Texas Instruments Design Review,* Aug. 7, 1991.

[24] J. A. Navarro, K. Chang, J. Tolleson, S. Sanzgiri, and R. Q. Lee, "A 29.3 GHz cavity enclosed aperture-coupled circular patch antenna for microwave circuit integration," *IEEE Microwave and Guided Wave Lett.,* vol. 1, no. 7, pp. 170–171, July 1991.

[25] M. V. Schneider, B. Glance, and W. F. Bodtmann, "Microwave and millimeter wave hybrid integrated circuits for radio systems," *Bell System Tech. J.,* pp. 1703–1726, July-Aug. 1969.

[26] J. A. Navarro and K. Chang, "Electronic beam steering of active antenna arrays," *Electron. Lett.,* vol. 29, no. 3, Feb. 4, 1993.

[27] J. A. Navarro, L. Fan, and K. Chang, "Active inverted stripline circular patch antennas for spatial power combining," *IEEE Trans. Microwave Theory Tech.,* vol. 41, no. 10, pp. 1856–1863, Oct. 1993.

[28] I. J. Bahl and P. Bhartia, *Microstrip Antennas.* Norwood, MA: Artech House, 1980.

[29] W. C. Chew and J. A. Kong, "Effect of fringing fields on the capacitance of a circular microstrip disk," *IEEE Trans. Microwave Theory Tech.,* vol. MTT-28, no. 2, pp. 98–104, Feb. 1980.

[30] M. Li, K. A. Hummer, and K. Chang, "Theoretical and experimental study of the input impedance of a cylindrical cavity-backed rectangular slot antenna," *IEEE Trans. Antennas Propagat.,* vol. 39, no. 8, pp. 1158–1166, Aug. 1991.

[31] V. F. Fusco, "Self-detection performance of active microstrip antennas," *Electron. Lett.,* vol. 28, no. 14, pp. 1362–1363, July 1992.

[32] R. A. York, "A new phase-shifterless beam-scanning technique using arrays of coupled oscillators," *IEEE Trans. Microwave Theory Tech.,* vol. 41, no. 10, pp. 1810–1815, Oct. 1993.

Julio A. Navarro (S'91–M'93) was born in Cordoba, Argentina on November 13, 1964. He received the B.S. and M.S. degrees in electrical engineering from Texas A&M University in 1988 and 1990, respectively. He is currently a Ph.D. candidate.

He was a cooperative education student with General Dynamics-Fort Worth from May 1985 to February 1991. At General Dynamics, he worked for Avionics Systems Design, Advanced Technology and Systems Engineering, Field Engineering, Emitters & Intelligence, Antenna Systems and Radar Cross-Section Research groups. At Texas A&M University, he has been a Research and Teaching Assistant since January 1991. His teaching assistant duties included Ultra-High Frequency Techniques course lab as well as many senior student projects. As a research assistant, he has introduced active endfire notch radiators, Gunn VCO's, and PIN switchable and varactor-tunable uniplanar filters. He has also introduced tunable slotline and CPW ring resonators. He has developed Ka-band aperture-coupled circular patch antennas for a NASA-Lewis/Texas Instruments-Mckinney project. He is currently working on active antenna elements for quasi-optical power combining in phased-arrays.

Kai Chang (S'75–M'76–SM'85–F'91) received the B.S.E.E. degree from the National Taiwan University, Taipei, Taiwan, the M.S. degree from the State University of New York at Stony Brook, and the Ph.D. degree from the University of Michigan, Ann Arbor, in 1970, 1972, and 1976, respectively.

From 1972 to 1976, he worked for the Microwave Solid-State Circuits Group, Cooley Electronics Laboratory of the University of Michigan as a Research Assistant. From 1976 to 1978, he worked with Shared Applications, Inc., Ann Arbor, where he worked in computer simulation of microwave circuits and microwave tubes. From 1978 to 1981, he worked for the Electron Dynamics Division, Hughes Aircraft Company, Torrance, CA, where he was involved in the research and development of millimeter-wave solid-state devices and circuits, power combiners, oscillators, and transmitters. From 1981 to 1985, he worked for the TRW Electronics and Defense, Redondo Beach, CA, as a Section Head, developing state-of-the-art millimeter-wave integrated circuits and subsystems including mixers, VCOs, transmitters, amplifiers, modulators, upconverters, switches, multipliers, receivers, and transceivers. He joined the Electrical Engineering Department of Texas A&M University in 1985 as an Associate Professor and was promoted to a Professor in 1988. In 1990, he was appointed E-Systems Endowed Professor of Electrical Engineering. His current interests are in microwave and millimeter-wave devices and circuits, microwave integrated circuits, microwave optical interactions, and antennas. He authored a book, *Microwave Solid-State Circuits and Applications* (New York: Wiley, 1994). He served as the editor of the four-volume *Handbook of Microwave and Optical Components* (New York: Wiley, 1989 and 1990). He is the editor of the *Microwave and Optical Technology Letters* and the *Wiley Book Series in Microwave and Optical Engineering.* He has published over 200 technical papers and several book chapters in the areas of microwave and millimeter-wave devices and circuits.

Dr. Chang received the Special Achievement Award from TRW in 1984, the Halliburton Professor Award in 1988, the Distinguished Teaching Award in 1989, and the Distinguished Research Award in 1992 from the Texas A&M University.